Available online at www.sciencedirect.com
SCIENCE DIRECT®
Journal of Sound and Vibration 263 (2003) 399–414
JOURNAL OF SOUND AND VIBRATION
www.elsevier.com/locate/jsvi

Mechanics and finite elements for the damped dynamic characteristics of curvilinear laminates and composite shell structures

T.S. Plagianakos, D.A. Saravanos*

Department of Mechanical Engineering and Aeronautics, University of Patras, Patras GR26500, Greece

Received 2 January 2002; accepted 23 May 2002

Abstract

Integrated mechanics and a finite element method are presented for predicting the damping of doubly curved laminates and laminated shell composite structures. Damping mechanics are formulated in curvilinear co-ordinates from ply to structural level and the structural modal loss factors are calculated using the energy dissipation method. The modelling of damping at the laminate level is based on first order shear shell theory. An eight-node shell damping finite element is developed. Comparisons of the present model with classical and discrete layer laminate damping theory predictions are shown. Modal damping and natural frequencies of composite plates and open cylindrical shells were measured and correlated with predicted results. Parametric studies illustrate the effect of curvature and lamination on modal damping and natural frequency.

1. Introduction

The importance of passive damping in improving the dynamic performance of flexible structures requiring tight vibration control, high fatigue endurance, impact resistance, aeroelastic stability and accurate positioning of devices and sensors is broadly recognized. Polymer–matrix composites are known to exhibit significantly higher material damping than most common metals, as a result of the polymer matrix and material heterogeneity. As a result, the development of analytical and computational models for the prediction and tailoring of passive damping in

*Corresponding author. Tel.: +30-61-996-191; fax: +30-61-997-234.
E-mail address: saravanos@mech.upatras.gr (D.A. Saravanos).

0022-460X/03/$ - see front matter
PII: S0022-460X(02)01059-3

composite structures with realistic geometries, such as wind turbine blades, fan blades, aircraft and automotive panels, is receiving current attention.

Substantial analytical and experimental work was reported on damping mechanisms of composite laminates, e.g., Refs. [1–5]. In the area of composite structures damping, Bicos and Springer [6] analyzed the damping of panels with cutouts. Alam and Asnani [7], Saravanos [8] and Taylor and Nayfeh [9] studied the vibrational characteristics of thick composite plates. Saravanos and Chamis [10] and Saravanos [11] presented single and discrete layer models and finite elements for laminated plates of variable thickness and lamination and predicted natural frequencies and modal loss factors. Saravanos and Pereira [12] presented analytical discrete layer solutions and a finite element for analyzing the effect of interply viscoelastic layers on the damping behaviour of plates. Zapfe and Lesieutre [13] and Maheri and Adams [14] developed finite element models to calculate damping in composite beams and plates, respectively, with interlaminar damping layers.

Some work limited in scope has been reported on the structural damping of composite shells, whereas very few experimental results have been presented. Singh and Gupta [15] reported a first order shear solution to calculate natural frequencies and damping in uni-directional composite shells. Chate et al. [16] developed a triangular finite element and predicted damping by the energy dissipation method for plates, shells and sandwich panels using a correspondence principle. Yet, it seems that neither mechanics and integrated damping models have been developed enabling unified predictions of damped dynamic characteristics of arbitrary laminated shells, nor a comprehensive study correlating analytical damping predictions with experimental values. Consequently, the present paper presents unified mechanics and a finite element formulation for predicting the damped vibrational characteristics of curvilinear composite shells of arbitrary geometry and lamination. Constitutive relations, equations of motion and first order shear kinematic assumptions are formulated in a curvilinear co-ordinate system. The formulation is applicable in both thin and intermediately thick shell structures. A special eight-node shell finite element incorporating the aforementioned damping mechanics is developed and validated with existing analytical results for beams and plates [8,11], as well as, with experimental results for beams [1], plates and curved shells. Vibration analysis experiments are conducted on glass/polyester (Gl/Pl) plates and cylindrical shells and measured modal damping is correlated with predicted results. The effect of lamination, boundary conditions and shell curvature on the modal damping of cylindrical shells is also studied.

2. Curvilinear laminate mechanics

A typical curvilinear doubly curved laminate configuration is shown schematically in Fig. 1. It is assumed that each ply of the laminate remains parallel to a reference curvilinear surface A_o, which is defined with respect to a global Cartesian co-ordinate system $Oxyz$. An orthogonal curvilinear co-ordinate system $O\xi\eta\zeta$ is considered, such that the axes ξ and η lie on the reference surface A_o, while the axis ζ remains straight and perpendicular to the layers of the laminate. Unless otherwise stated, all material properties, displacements and strains refer to the curvilinear co-ordinate system.

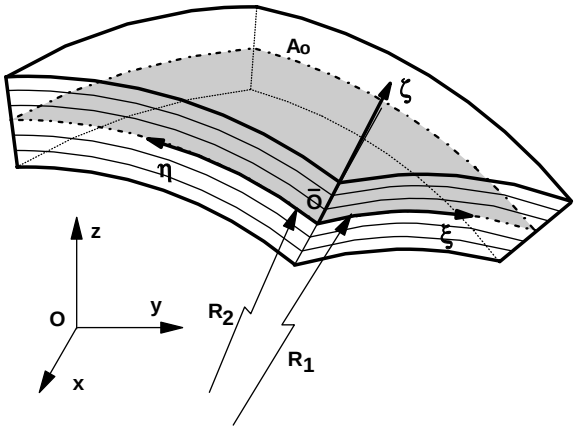

Fig. 1. Curvilinear laminate with co-ordinate systems.

2.1. Governing material equations

Each ply is assumed to have viscoelastic behaviour. Assuming cyclic loading, the off-axis complex stress component $\boldsymbol{\sigma}_c$ is provided by

$$\boldsymbol{\sigma}_c = ([\mathbf{Q}_c] + \mathrm{j}[\mathbf{Q}_c][\boldsymbol{\eta}_c])\mathbf{S}_c, \tag{1}$$

where $\mathbf{S}_c$, $\boldsymbol{\sigma}_c$ are the engineering strain and stress in extended vectorial notation, $[\mathbf{Q}_c]$ is the storage stiffness matrix and $[\boldsymbol{\eta}_c]$ is the damping matrix, j is the imaginary unit, subscript c indicates that the previous quantities are defined with respect to the axes of the curvilinear system $O\xi\eta\zeta$.

On-axis ply damping: The material co-ordinate system indicated with subscript l is curvilinear with axis 1 parallel to the fibers and through-thickness axis 3 parallel to axis ζ. It is assumed that the damping of the composite ply on the material co-ordinate system is orthotropic (in planes 1–2 and 1–3), described by six damping (loss) coefficients, these are [4]: (1) longitudinal loss coefficient, η_{l1} (direction 11); (2) transverse in-plane loss coefficient, η_{l2} (direction 22); (3) transverse through the thickness loss coefficient, η_{l3} (direction 33); (4) in-plane shear loss coefficient, η_{l6} (direction 12); (5) interlaminar shear loss coefficient, η_{l4} (direction 23); and (6) interlaminar shear loss coefficient, η_{l5} (direction 13). Further, transverse isotropy is assumed on the 2–3 plane, which reduces the independent coefficients to four ($\eta_{l3} = \eta_{l2}$, $\eta_{l5} = \eta_{l6}$). The damping coefficients form the on-axis ply damping matrix $[\boldsymbol{\eta}_l]$:

$$[\boldsymbol{\eta}_l] = \begin{bmatrix} \eta_{l1} & 0 & 0 & 0 & 0 & 0 \\ 0 & \eta_{l2} & 0 & 0 & 0 & 0 \\ 0 & 0 & \eta_{l3} & 0 & 0 & 0 \\ 0 & 0 & 0 & \eta_{l4} & 0 & 0 \\ 0 & 0 & 0 & 0 & \eta_{l5} & 0 \\ 0 & 0 & 0 & 0 & 0 & \eta_{l6} \end{bmatrix}. \tag{2}$$

Off-axis ply damping: For the case of rotated (off-axis) curved plies, the equivalent damping capacity of the composite in the curvilinear co-ordinate system $O\xi\eta\zeta$ is best described by the

following (6×6) off-axis damping matrix $[\boldsymbol{\eta}_c]$ [4] provided by the following transformation:

$$[\boldsymbol{\eta}_c] = [\mathbf{R}]^{\mathrm{T}}[\boldsymbol{\eta}_l][\mathbf{R}]^{-\mathrm{T}}, \tag{3}$$

where η indicates loss factor.The off-axis ply damping matrix is non-diagonal and has the general form

$$[\boldsymbol{\eta}_c] = \begin{bmatrix} \eta_{c11} & \eta_{c12} & 0 & 0 & 0 & \eta_{c16} \\ \eta_{c21} & \eta_{c22} & 0 & 0 & 0 & \eta_{c26} \\ 0 & 0 & \eta_{c33} & 0 & 0 & 0 \\ 0 & 0 & 0 & \eta_{c44} & \eta_{c45} & 0 \\ 0 & 0 & 0 & \eta_{c54} & \eta_{c55} & 0 \\ \eta_{c61} & \eta_{c62} & 0 & 0 & 0 & \eta_{c66} \end{bmatrix}. \tag{4}$$

Strain–displacement relations: The strain $\mathbf{S}_c$ in the curvilinear co-ordinate system of a shallow laminate is related to the displacements as follows:

$$\begin{aligned} S_1 &= \frac{1}{g_{11}^0}\left(u_{,\xi} + \frac{g_{11,\eta}^o}{g_{22}^o}v + \frac{g_{11}^o}{R_1}w\right), \\ S_2 &= \frac{1}{g_{22}^0}\left(v_{,\eta} + \frac{g_{22,\xi}^o}{g_{11}^o}v + \frac{g_{22}^o}{R_2}w\right), \\ S_6 &= \frac{1}{g_{11}^o}\left(v_{,\xi} - \frac{g_{11,\eta}^o}{g_{22}}u\right) + \frac{1}{g_{22}^o}\left(u_{,\eta} - \frac{g_{22,\xi}^o}{g_{11}^o}v\right), \\ S_3 &= w_{,\zeta}, \\ S_4 &= v_{,\zeta} + \frac{1}{g_{22}^0}\left(w_{,\eta} - \frac{g_{22}^o}{R_2}v\right), \\ S_5 &= u_{,\zeta} + \frac{1}{g_{11}^0}\left(w_{,\xi} - \frac{g_{11}^o}{R_1}u\right), \end{aligned} \tag{5a–f}$$

where u, v, w are the displacements along ξ, η and ζ, respectively, R_1 and R_2 are the curvature radii of the surface A_o along the orthogonal axes ξ and η respectively, and g_{ij}^o are the metric tensor components corresponding to the reference surface A_o.

2.2. Kinematic assumptions

A first order shear theory is used to model the variation of the displacement through the thickness of the shell. The displacements take the following form:

$$\begin{aligned} u(\xi,\eta,\zeta,t) &= u^o(\xi,\eta,t) + \zeta\beta_\xi(\xi,\eta,t), \\ v(\xi,\eta,\zeta,t) &= v^o(\xi,\eta,t) + \zeta\beta_\eta(\xi,\eta,t), \\ w(\xi,\eta,\zeta,t) &= w^o(\xi,\eta,t), \end{aligned} \tag{6}$$

where again u°, v^o and w° are the displacements (on the reference surface A_o) along ξ, η and ζ axes respectively, β_ξ and β_η are the rotation angles. In the context of Eq. (5), the generalized strains are

the mid-strains $\mathbf{S}^0$ on the doubly curved reference surface A_o:

$$S_1^o = \frac{1}{g_{11}^o}\left(u_{,\xi}^o + \frac{g_{11,\eta}^o}{g_{22}^o} v^o\right) + \frac{w^o}{R_1}, \quad S_2^o = \frac{1}{g_{22}^o}\left(v_{,\eta}^o + \frac{g_{22,\xi}^o}{g_{11}^o} u^o\right) + \frac{w^o}{R_2},$$
$$S_6^o = \frac{1}{g_{11}^o}\left(v_{,\xi}^o - \frac{g_{11,\eta}^o}{g_{22}} u^o\right) + \frac{1}{g_{22}^o}\left(u_{,\eta}^o - \frac{g_{22,\xi}^o}{g_{11}} v^o\right),$$
$$S_4^o = \beta_\eta + \frac{w_{,\eta}^o}{g_{22}^o} - \frac{v^o}{R_2}, \quad S_5^o = \beta_\xi + \frac{w_{,\xi}^o}{g_{11}^o} - \frac{u^o}{R_1} \tag{7}$$

and the curvatures $\mathbf{k}$, with components defined as follows:

$$k_1 = \frac{1}{g_{11}^o}\left(\beta_{\xi,\xi} + \frac{g_{11,\eta}^o}{g_{22}^o}\beta_\eta\right), \quad k_2 = \frac{1}{g_{22}^o}\left(\beta_{\eta,\eta} + \frac{g_{22,\xi}^o}{g_{11}^o}\beta_\xi\right),$$
$$k_6 = \frac{1}{g_{11}^o}\left(\beta_{\eta,\xi} - \frac{g_{11,\eta}^o}{g_{22}^o}\beta_\xi\right) + \frac{1}{g_{22}^o}\left(\beta_{\xi,\eta} - \frac{g_{22,\xi}^o}{g_{11}^o}\beta_\eta\right). \tag{8}$$

2.3. Laminate damping

The dissipated strain energy per unit area in the laminate ΔW_L during a vibration cycle is defined as follows:

$$\Delta W_L = 1/2|\mathbf{J}| \int_{-h/2}^{h/2} \mathbf{S}_c^{\mathrm{T}}[\mathbf{Q}_c][\boldsymbol{\eta}_c]\mathbf{S}_c \, \mathrm{d}\zeta, \tag{9}$$

where $|\mathbf{J}| = g_{11}^o g_{22}^o$ is the determinant of the Jacobean of the Cartesian to the curvilinear coordinates.

Again, taking into account Eq. (6) and integrating through the thickness, the dissipated strain energy per unit area of the laminate is

$$\Delta W_L = \tfrac{1}{2}[S_i^o A_{dij} S_j^o + k_i B_{dij} S_j^o + S_i^o B_{dij} k_j + k_i D_{dij} k_j + S_\kappa^o A_{d\kappa\lambda} S_\lambda^o],$$
$$i,j = 1,2,6, \quad \kappa,\lambda = 4,5, \tag{10}$$

where $[\mathbf{A}_d]$, $[\mathbf{B}_d]$, $[\mathbf{D}_d]$ are the extensional, extensional-bending and bending damping matrices, respectively, and $[\mathbf{A}_{sd}]$ is the transverse shear damping matrix, defined as

$$\langle A_{dij}, B_{dij}, D_{dij} \rangle = g_{11}^o g_{22}^o \sum_{k=1}^{L} \int_{\zeta_k}^{\zeta_{k+1}} Q_{c_{ik}} \boldsymbol{\eta}_{c_{kj}} \langle 1, \zeta, \zeta^2 \rangle \, \mathrm{d}\zeta, \quad i,j,k = 1,2,6,$$
$$A_{sdij} = g_{11}^o g_{22}^o \sum_{k=1}^{L} \int_{\zeta_k}^{\zeta_{k+1}} Q_{c_{ik}} \boldsymbol{\eta}_{c_{kj}} \, \mathrm{d}\zeta, \quad i,j,k = 4,5. \tag{11}$$

No shear correction factor is assumed in this work for Eq. (11). The previous expression is complete in that it represents general laminate configurations and deformations. Therefore, the

equivalent damping capacity of a general curvilinear laminate is a function of the laminate parameters and the specific deformation state.

3. Structural mechanics

In this section the finite element developed is described, equations of motion are presented and the energy approach is used for the calculation of the damping capacity of the structure.

3.1. Equations of motion

Equations of motion are defined in the orthogonal curvilinear system in standard variational form

$$-\int_V \delta S_i \sigma_i |\mathbf{J}|\,\mathrm{d}V + \int_V \delta u_\kappa(-\rho\ddot{u}_\kappa)|\mathbf{J}|\,\mathrm{d}V + \int_{\Gamma_\sigma} \delta u_\kappa \tau_\kappa\,\mathrm{d}\Gamma = 0,$$
$$i,j = 1,...,6, \quad \kappa = 1,...,3, \tag{12}$$

where the three integrals on the left-hand side express variation of strain energy of the structure, work of body forces and work of surface tractions, respectively.

3.2. Finite element formulation

Based on the previous generalized equations, an eight-node finite element was used with bi-quadratic shape functions of the Serendipity family. Approximations of the generalized mechanical state (displacements and rotation angles) of the reference surface are of the following type:

$$\begin{aligned} u_j^o(\xi,\eta,t) &= \textstyle\sum_{i=1}^{M} u_j^{oi}(t) N^i(\xi,\eta), \quad j = 1,...,3, \\ \beta_j^o(\xi,\eta,t) &= \textstyle\sum_{i=1}^{M} \beta_j^{oi}(t) N^i(\xi,\eta), \quad j = 1,2. \end{aligned} \tag{13}$$

The radii R_1 and R_2 and the metric coefficients g_{11}^o, g_{22}^o of the reference surface are calculated in each element based on the previous iso-parametric surface representation.

Assuming harmonic motion and substituting the previous Eqs. (11) and (13) into the equations of motion (12), integrating over the shell area of each element, and collecting the common coefficients we arrive to the final form of an N-size discrete system of equations describing the forced frequency response of the shell

$$-\omega^2[\mathbf{M}]\mathbf{U} + \mathrm{j}[\mathbf{C}]\mathbf{U} + [\mathbf{K}]\mathbf{U} = \mathbf{F}(\omega), \tag{14}$$

where [**M**],[**C**] and [**K**] are the inertia, damping and stiffness matrices of the structure, respectively.

3.3. Structural damping

Solution of Eqs. (14) for the free vibration case ($\mathbf{F} = 0$) yields the damped complex conjugate eigenvalues (poles) of the system. Alternatively, using the dissipated energy approach [4], the modal loss factor associated with the mth order mode η_m of the laminated shell will be the ratio of

dissipated to maximum strain modal energy

$$\eta_m = \frac{\int_A \Delta W_{Lm}\, \mathrm{d}A}{\int_A W_{Lm}\, \mathrm{d}A}, \tag{15}$$

where ΔW_{Lm}, W_{Lm} are, respectively, the dissipated and maximum laminate strain energies of the mth undamped mode shape. Numerical solution of the undamped case ($[\mathbf{C}]=0$) in Eq. (14) provides the undamped natural frequencies of the shell structure and the modal displacement vectors. The modal loss factor is then

$$\eta_m = \frac{\mathbf{U}_m^{\mathrm{T}}[\mathbf{C}]\mathbf{U}_m}{\mathbf{U}_m^{\mathrm{T}}[\mathbf{K}]\mathbf{U}_m}. \tag{16}$$

4. Experiments

Modal analysis experiments were conducted on a $[0^0]$ Gl/Pl plate and a $[0^0]$ Gl/Pl cylindrical panel with fibres aligned along the circumferential direction. Both components were fabricated using hand lay-up and tested under free–free boundary conditions in order to eliminate damping due to friction in the supports. Similar experiments were performed on uni-directional beam specimens to measure ply damping coefficients and elastic constants.

Experimental configuration: The experimental set-up is shown schematically in Fig. 2. An instrumented impact hammer with a load cell was used to excite the structure at positions 1 (plate) or 3 (panel). The acceleration of the structure was measured using an 1gr accelerometer at the middle of the plate (position 1), and at the corner of the cylindrical panel (position 2). The positions of excitation and acceleration measurement were chosen such that a high number of modes could be acquired within the respective frequency response functions (FRFs). The signals of the impact hammer and the accelerometer were first amplified, then digitized through a high-speed data acquisition board and finally processed using FFT software, to obtain power spectra and FRFs of the accelerance (acceleration/force) of the tested component. The measured FRFs were used to extract the modal damping and frequency values of each vibration mode. For this reason, the measured FRFs were further correlated with the ones generated by a known parametric model consisting of a series of complex exponential terms, each term approximating an individual mode with known modal parameters (frequency and damping), such that the least-squares error between the model and measured FRFs was minimized. Through this correlation, the modal frequencies and damping coefficients of the tested specimen or structure were extracted.

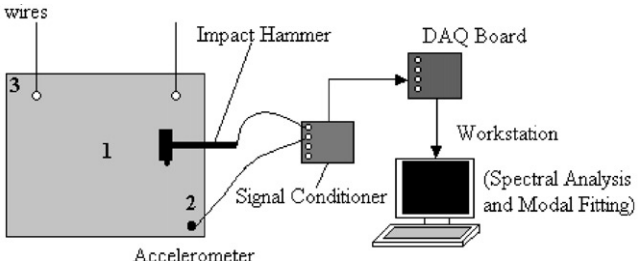

Fig. 2. Experimental configuration for measurement of natural frequency and modal damping.

5. Applications and discussion

Modal damping capacities and natural frequencies of various beam, plate and shell composite structures were predicted using the present methodology. Results were compared with reported experimental data, as well as, with other analytical solutions obtained with classical laminate damping theory (CLDT) and discrete layer damping theory (DLDT) Ritz solutions. Additional results were correlated with measured values obtained from experiments conducted on a Gl/Pl plate and a cylindrical panel. Finally, the effect of boundary conditions and lamination on shell damping was studied.

5.1. Materials and assumptions

The composite materials considered were graphite/epoxy (Gr/epoxy) of 50% fiber volume ratio [1] and Gl/Pl. The mechanical properties of Gr/epoxy are shown in Table 1. The tested plate and cylindrical shell panel were made of Gl/Pl composite. The damping and elastic properties of Gl/Pl were calculated from measurements of natural frequency and modal damping in off-axis unidirectional composite beam specimens of [0], [15], [30], [45], [60], [75] and [90] fiber orientation angle [17], under free support. The specimens were cut from the $[0^0]$ plate after it was tested. Free flexure conditions were assumed for the beam specimens ($N_x \neq 0$, $M_x \neq 0$, $N_y = N_s = M_y = M_s = 0$). It is also pointed out that the damping values of higher modes may include contribution from shear terms (see Figs. 4 and 5). To avoid this problem, the beam specimens had a very high thickness aspect ratio ($L/h = 200$) to ensure that shear effects on the first modes remained minimal. For the calculation of the elastic properties of the composite (E_{11}, E_{22}, G_{12}, v_{12}) the equivalent elasticity modulus was fitted to experimental values backcalculated from the measured modal frequencies of each beam. Whereas for the damping properties (η_{l1}, η_{l2}, η_{l6}) the flexural damping capacity was fitted to the measured modal damping of the bending modes of the specimens. The values shown in Table 1 correspond to measured data in the high-frequency range (>150 Hz), where frequency effects on damping were observed to be insignificant.

$[0/90/\pm 45]_S$ *Free–free beam*: Fig. 3 shows predicted modal damping values of the fundamental mode of a $[\theta/90+\theta/45+\theta/-45+\theta]_S$ Gr/epoxy free–free thin beam ($l/h = 125$), as a function of fiber orientation angle θ. The beam was 200 mm long, 12 mm wide and 1.6 mm thick. It was modelled using a 10×1 uniform mesh. Measured [1] and predicted results using CLDT [11] are also shown. The FSDT predictions are in very good agreement with CLDT, because the beam is thin, yet slightly better than those of CLDT towards the reported measurements. As seen in Fig. 3,

Table 1
Elastic and damping properties of HM-S/DX210 Gr/epoxy and Gl/Pl composite

Composite	ρ (kg/m^3)	E_{11} (GPa)	E_{22} (GPa)	G_{12} (GPa)	G_{23} (GPa)	v_{12}	η_{l1} (%)	η_{l2} (%)	η_{l4} (%)	η_{l6}(%)
Gr/epoxy	1588	192.3	5.05	3.12	2.03	0.275	0.08	0.67	0.76	1.11
Gl/Pl	1672	25.8	8.7	3.5	3.5*	0.34	0.65	1.70	0	2.05

*Not measured.

the deviation between CLDT and FSDT is higher in laminations, where the interlaminar shear effects are higher, for example when $\theta = 45^{\circ}$.

$[0_4/90_4]_S$ *Simply supported plate*: Figs. 4 and 5 demonstrate the effect of thickness aspect ratio on the normalized natural frequencies and modal loss factors of the fundamental and higher

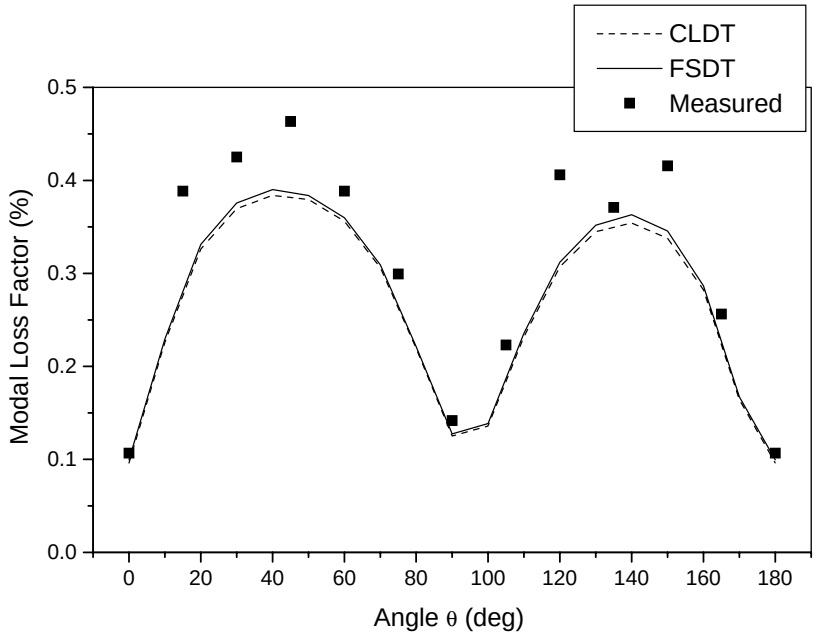

Fig. 3. First modal damping of a $[\theta/90 + \theta/45 + \theta/ - 45 + \theta]_S$ Gr/epoxy free–free beam.

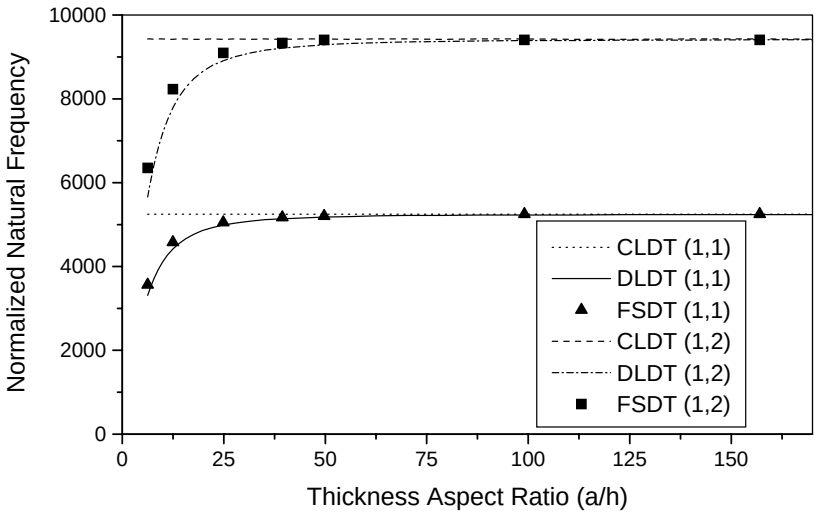

Fig. 4. Effect of thickness aspect ratio on the natural frequency of a $[04/904]_S$ Gr/epoxy simply supported plate. Numbers in parenthesis indicate bending mode shape.

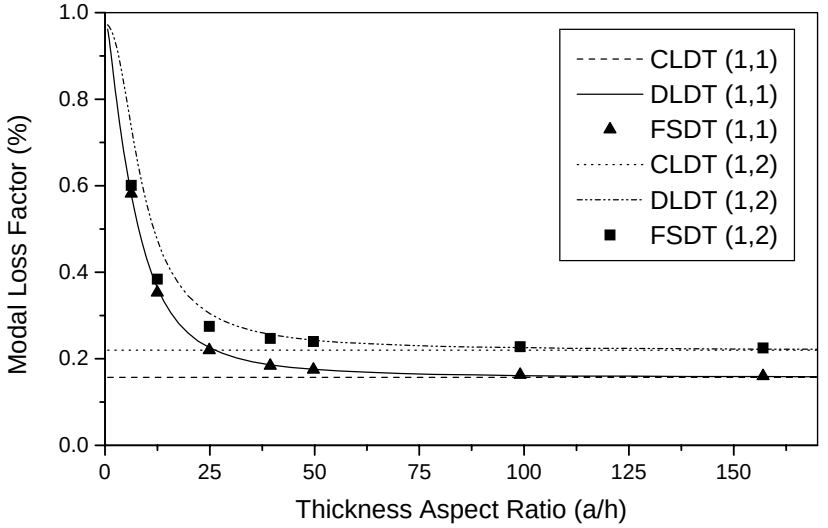

Fig. 5. Effect of thickness aspect ratio on the modal loss factor of a $[04/904]_S$ Gr/epoxy simply supported plate. Numbers in parenthesis indicate bending mode shape.

bending modes (1, 1) and (1, 2), respectively, of a simply supported square plate $[0_4/90_4]_S$, having an edge length of 406.4 mm. The natural frequencies were normalized by $\omega_{norm} = \omega a^2/h$. A uniform (8×8) mesh was used. Results are also shown from an exact Ritz solution using DLDT with $N = 16$ layers, which has shown to provide robust predictions of damping capturing all interlaminar shear effects through-thickness [8]. Clearly, the FSDT element provided superior estimates of modal frequency and damping than the CLDT exact Ritz solution in thick, intermediately thick and thin plates due to its ability to capture an average interlaminar shear strain and approaches the exact DLDT solution. The difference between the CLDT exact Ritz solution and DLDT predictions of the modal loss factor provide an average estimation of interlaminar shear damping. Finally, the results of the FSDT finite element converge to the exact CLDT and DLDT solutions as the plate thickness is decreased, indicating excellent behaviour of the damping element at low thicknesses and no shear locking.

$[0_3]$ Gl/Pl free–free plate: The tested square plate with dimensions 455 mm × 455 mm × 2.3 mm was modelled using a uniform (8×8) mesh. Fig. 6 illustrates the FE predicted and measured frequencies and modal loss factors. The correspondence of the modes has been carried out after careful inspection of mode shapes (FE) and modal loss factors. Very good agreement was obtained between predicted and experimental data for both natural frequency and modal loss factor. The plate was fabricated using hand lay-up, resulting in some imperfections, which are in part responsible for the deviations observed.

$[0_3]$ Gl/Pl free–free cylindrical panel: The tested panel was 0.355 mm long (circumferential direction), 204 mm wide and 3.3 mm thick. A finer mesh along the circumferential direction (16×4) was used. Fig. 7 illustrates the FE predicted and experimentally measured values of modal loss factors versus modal frequencies. Very good agreement was obtained between predicted and measured natural frequencies and modal loss factors. Deviations are higher for modal damping, since it is a more sensitive quantity to local imperfections due to hand lay-up fabrication, but there

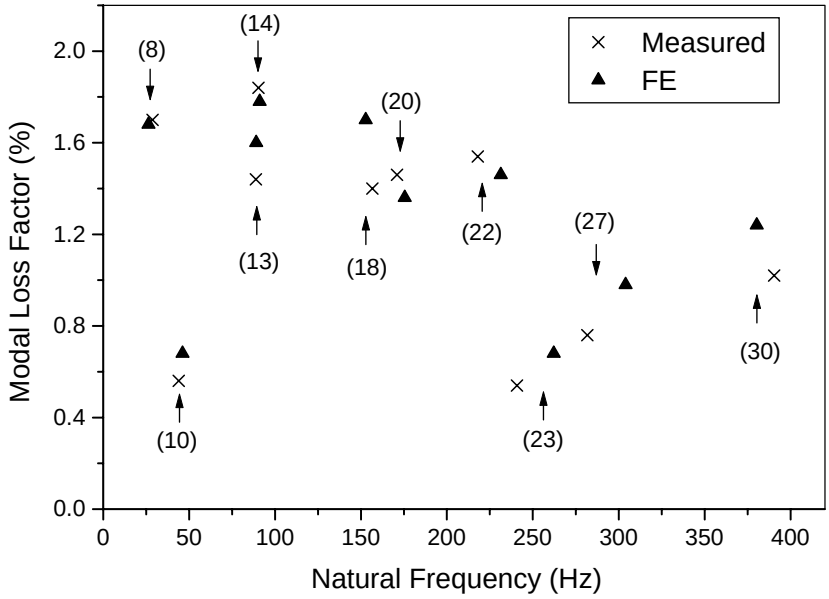

Fig. 6. FE and measured values for natural frequency and modal loss factor of a UD Gl/Pl free–free plate. Numbers in parenthesis indicate predicted mode number.

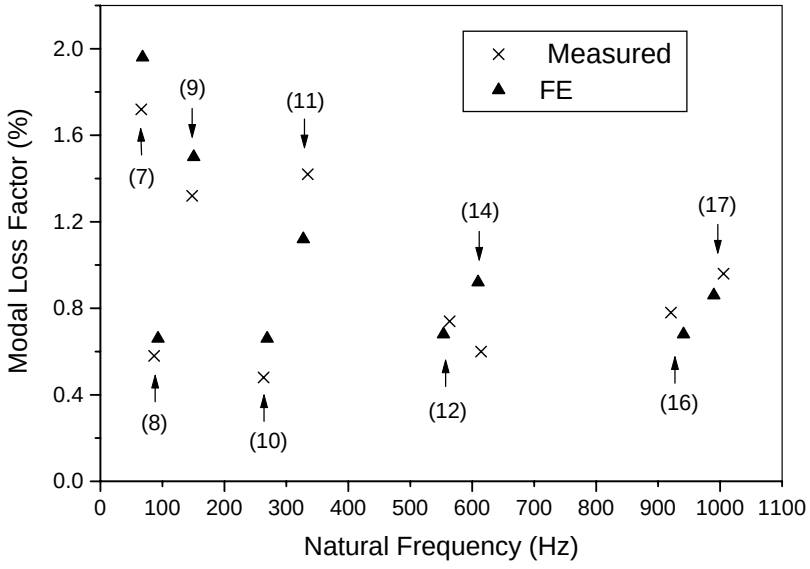

Fig. 7. FE and measured values for natural frequency and modal loss factor of a UD Gl/Pl free–free cylindrical panel. Numbers in parenthesis indicate predicted mode number.

is still good correlation between predicted and experimental results. These successful correlations lend further credence to the capability of the method to provide reliable predictions on natural frequency and modal loss factor in thin and intermediately thick shell structures.

$[0_4/90_4]_S$ Simply supported cylindrical panel: The effect of curvature on natural frequency and modal damping of a composite cylindrical shell panel with a constant circumferential length of 406.4 mm (circumferential direction), constant axial length (width) of 406.4 mm and uniform thickness of 2.7 mm was investigated. A uniform (15×4) FE mesh was implemented. Figs. 8 and 9 show the effect of curvature on the natural frequencies of the fundamental and higher bending modes (1,1) and (2,2) and on the corresponding modal loss factors. The natural frequencies

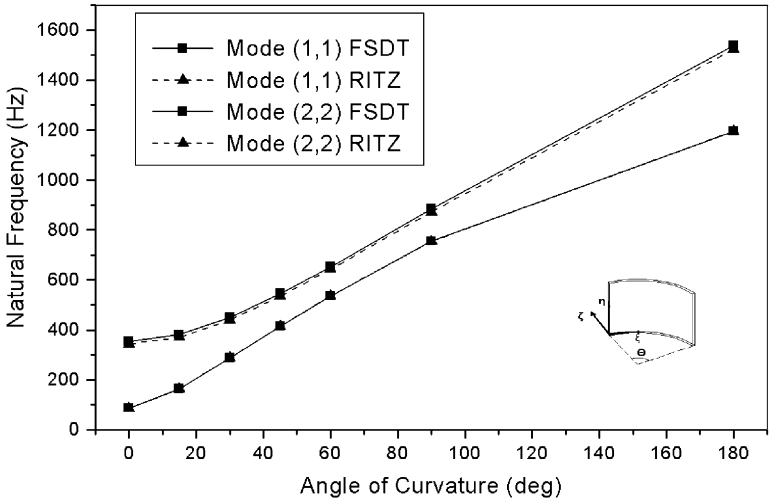

Fig. 8. Effect of curvature angle on the fundamental bending frequencies of a $[04/904]_S$ Gr/epoxy simply supported shell panel. Numbers in parenthesis indicate bending mode shape.

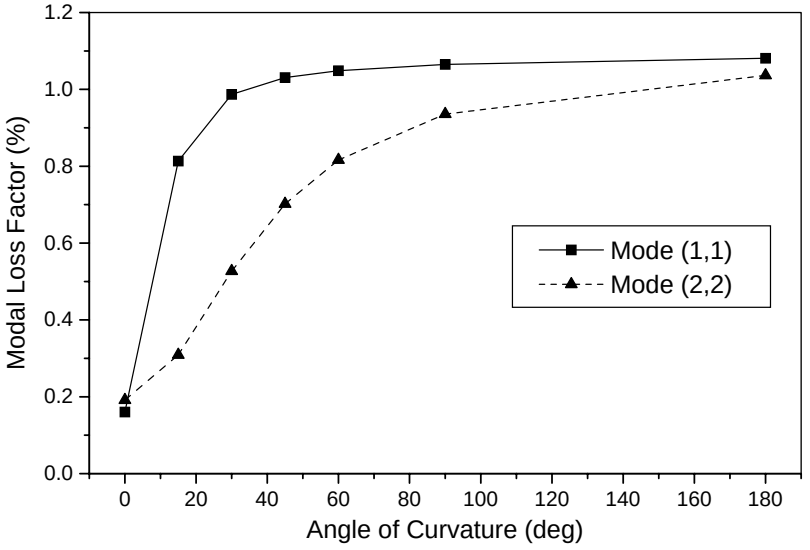

Fig. 9. Effect of curvature angle on modal loss factors (1, 1) and (2, 2) of a $[04/904]_S$ Gr/epoxy simply supported shell panel. Numbers in parenthesis indicate bending mode shape.

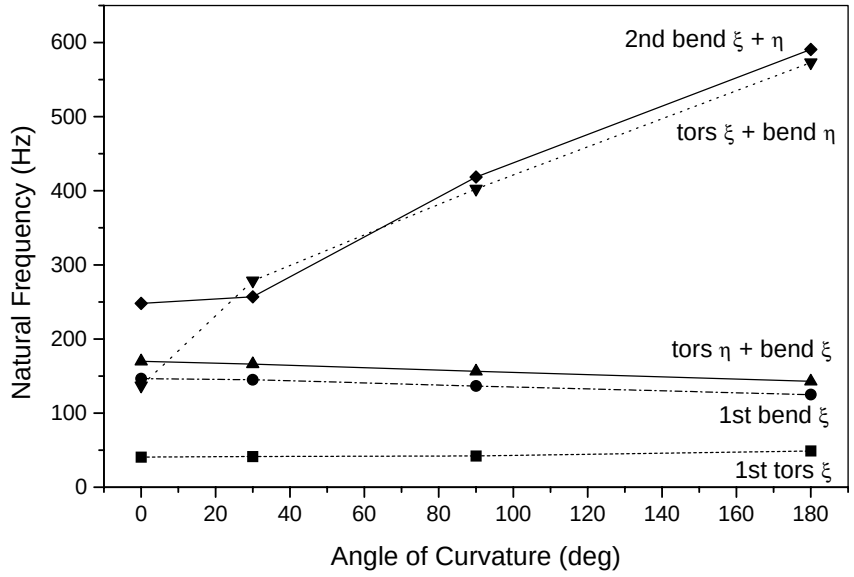

Fig. 10. Effect of curvature angle on natural frequencies of a $[0/90/\pm 45]_S$ Gr/epoxy free–free shell panel (ξ hoop, η axial direction).

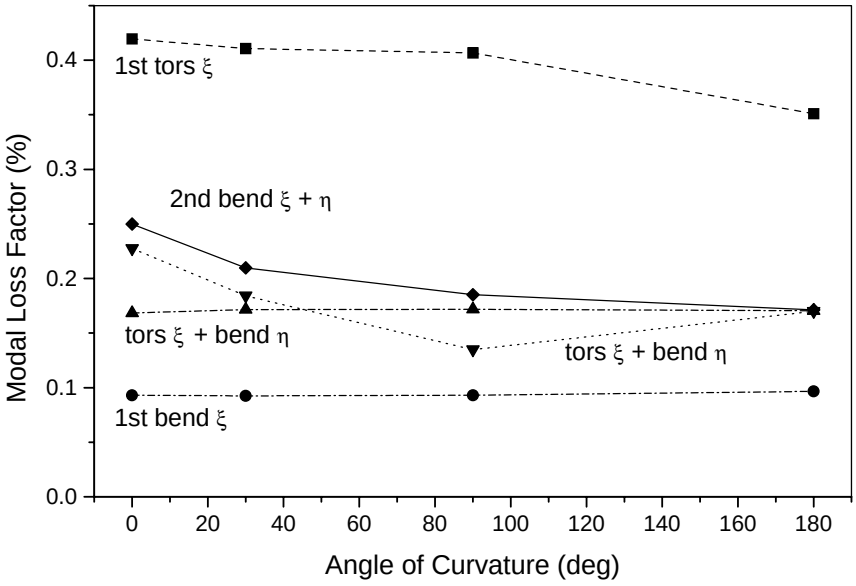

Fig. 11. Effect of curvature angle on modal loss factors of a $[0/90/\pm 45]_S$ Gr/epoxy free–free shell panel (ξ hoop, η axial direction).

resulting from the first order shear damping theory approach are compared with an exact Ritz solution with excellent agreement. Both quantities ω and η increased with curvature for both modes studied. A significant portion of damping is in-plane (shear) damping induced

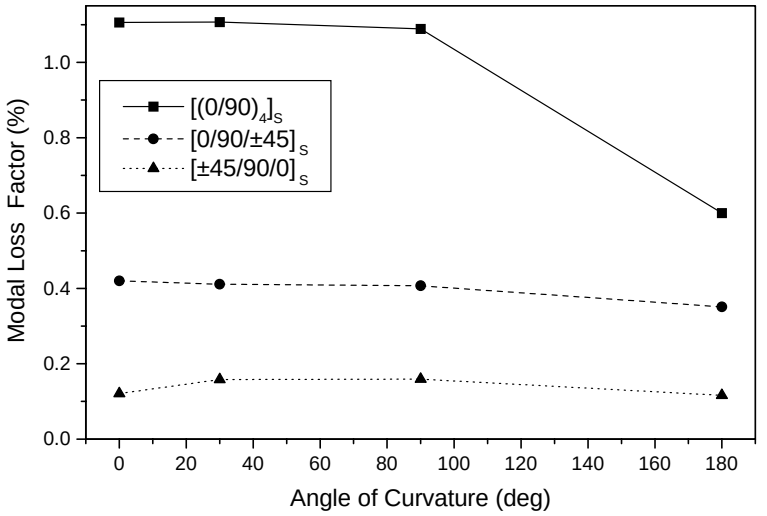

Fig. 12. Effect of curvature angle on modal loss factor of the first torsional mode in three different laminations (ξ hoop, η axial direction).

through geometric membrane–flexure coupling. This point will be further illustrated in the following cases.

Free–free cylindrical panels: Figs. 10 and 11 illustrate the effect of curvature angle on natural frequencies and corresponding modal loss factors of a $[0/90/\pm 45]_S$ free–free cylindrical panel with identical dimensions as the one used in previous case. Due to the complexity of the mode shapes they are referred as torsion, torsion and bending, etc. in the direction they appear. As expected, natural frequencies are lower than those in the simply supported case. In the current case, ω and η show an opposite trend as the curvature increases, which indicates that the boundary conditions strongly influence the modal damping capacity of the structure. The effect of lamination on the modal damping of the first torsional mode is shown in Fig. 12 for three different laminations ($[(0/90)_4]_S$, $[(0/90/\pm 45)]_S$, $[(\pm 45/90/0)]_S$) as a function of curvature angle. It is apparent that the third lamination has the lowest modal loss factor in this particular mode, due to increased stiffness and reduced damping in the maximum shear direction.

6. Summary

The mechanics and a finite element-based formulation for predicting modal damping and natural frequencies of curvilinear composite shell structures were presented. Damping mesomechanics were formulated in curvilinear co-ordinates using first order shear kinematics. An eight-node shell damping element was developed and modal loss factors were calculated by the energy dissipation method.

Numerical results were presented for composite beam, plates and cylindrical panels. Experiments were also conducted to provide measured modal damping data for composite plates and cylindrical panels, not previously existing in open literature. Comparisons with other reported

damping theories illustrated that the present model accurately captures the damping of thin shells and that it also yields very good predictions for thicker laminates. Moreover, correlations with reported experimental results and with new experimental data further quantified the ability of the present methodology to predict natural frequency and modal damping in thin and intermediately thick shell structures. The effect of curvature on modal damping and natural frequency was also illustrated; in free–free shell panels damping and frequency follow an opposite trend as the curvature increases, whereas for simply supported boundary conditions both quantities increased drastically for the lamination studied. The effect of lamination was also investigated in the free–free case. Future studies will include direct prediction of damping from the equations of motion, as well as, studies on the enhancement of damping in curved shell structures.

Acknowledgements

Part of this work was supported by ENK6-CT2000-00320 ENERGIE program. Materials and specimens were provided by Mr. Theodore Kossivas of Geoviologiki SA. This support is gratefully acknowledged by the authors. The authors want also to thank Aeronautical Engineer Nikos Chrisochoidis for assisting with the experimental work.

References

[1] R.G. Ni, R.D. Adams, The damping and dynamic moduli of symmetric laminated composite beams—theoretical and experimental results, Journal of Composite Materials 18 (2) (1984) 104–121.
[2] R.F. Gibson, R. Plunkett, Dynamic mechanical behaviour of fiber-reinforced composites: measurements and analysis, Journal of Composite Materials 10 (1976) 325–341.
[3] S. Yang, R.F. Gibson, Integration of vibration testing and finite-element analysis for estimating dynamic mechanical properties of cantilever-beam samples, Experimental Techniques 20 (6) (1996) 21–24.
[4] D.A. Saravanos, C.C. Chamis, Mechanics of damping for fiber composite laminates including hygro-thermal effects, American Institute of Aeronautics and Astronautics Journal 28 (10) (1990) 1813–1819.
[5] C.G. Wren, V.K. Kinra, Axial damping in metal–matrix composites I: a theoretical model and its experimental verification, Experimental Mechanics 32 (2) (1992) 172–178.
[6] S. Bicos, G.S. Springer, Vibrational characteristics of composite panels with cutouts, American Institute of Aeronautics and Astronautics Journal 27 (8) (1989) 1116–1122.
[7] N. Alam, N.T. Asnani, Vibration and damping analysis of fibre reinforced composite material plates, Journal of Composite Materials 20 (1) (1986) 2–18.
[8] D.A. Saravanos, Integrated damping mechanics for thick composite laminates and plates, Journal of Applied Mechanics 61 (2) (1994) 375–383.
[9] T.W. Taylor, A.H. Nayfeh, Damping characteristics of laminated thick plates, Journal of Applied Mechanics 64 (1) (1997) 132–138.
[10] D.A. Saravanos, C.C. Chamis, Computational simulation of damping in composite structures, Journal of Reinforced Plastic and Composites 10 (3) (1991) 256–278.
[11] D.A. Saravanos, Analysis of passive damping in thick composite structures, American Institute of Aeronautics and Astronautics Journal 31 (8) (1993) 1503–1510.
[12] D.A. Saravanos, J.M. Pereira, Effects of interply damping layers on the dynamic characteristics of composite plates, American Institute of Aeronautics and Astronautics Journal 30 (12) (1992) 2906–2913.
[13] J.A. Zapfe, G.A. Lesieutre, A discrete layer beam finite element for the dynamic analysis of composite sandwich beams with integral damping layers, Computers & Structures 70 (2) (1999) 647–666.

[14] M.R. Maheri, R.D. Adams, Finite element prediction of modal response of damped layered composite panels, Composites Science and Technology 55 (1) (1995) 13–23.
[15] S.P. Singh, K. Gupta, Damped free vibrations of layered composite cylindrical shells, Journal of Sound and Vibration 172 (2) (1994) 191–209.
[16] K. Chate, R. Rikards, A. Korjakin, Analysis of free damped vibrations of laminated composite cylindrical shells, Mechanics of Composite Materials 31 (5) (1995) 474–485.
[17] N. Chrisochoidis, Measurement of Damping Coefficients of Glass/Polyester Composites, M.S. Thesis, Department of Mechanical Engineering and Aeronautics, University of Patras, Greece, 2001.